THE EFFECT OF NOISE ON THE ACCURACY OF STRAIN MEASURMENT WHEN USING STRAIN ENCODED (SENC) MRI

T. Yousef[1], N. F. Osman[2]

[1]Department of Electrical Engineering, Johns Hopkins University, Baltimore, MD, United States, [2]Department of Radiology, Johns Hopkins University, Baltimore, MD, United States

Introduction: Imaging the contractility of the myocardium is one of the advantages of MR modality. Strain encoding (SENC) was developed as a modification to the MR tagging pulse sequence so that the changes in tags spacing, which relates to regional strain in the through plane direction, appears immediately on the MR images.

Theory: In SENC, The acquired images are modified by adding a gradient moment in the slice-selection direction to cause demodulation with a specific spatial frequency, which is called the *tuning* frequency [1]. Two Images I_L and I_H are acquired for two different tuning frequencies, and the local strain in a pixel located at a location y and time t can be computed as [1]:

$$\tilde{\varepsilon}(y;t) = \frac{\Delta\omega(y;t)}{\tilde{\omega}(y;t)} = \left(\frac{\omega_0}{\tilde{\omega}(y;t)} - 1\right), \tilde{\omega}(y;t) = \frac{\omega_L I(y;t;\omega_L) + \omega_H I(y;t;\omega_H)}{I(y;t;\omega_L) + I(y;t;\omega_H)}, (1)$$

a. **Strain Range:** In order to measure strain properly, the corresponding change in local spatial frequency of the tags has to be within the range between the low- and high-tuning frequencies. A good representation of the shifts in tag frequency due to local strain can be represented as shifts in the harmonic peak in the K_z direction, as shown in Fig 1. For that reason, the width of the harmonic peak in the frequency domain (B=1/SliceThickness), which depends on the slice thickness, must be considered. The maximum allowable strain range is bound by the maximum allowable shifts on both directions while taking into account that the peak should always lie between ω_L and ω_H (which is a basic assumption for the used center of gravity methodology [1]) and that ω_L and ω_H do not lie outside the slice profile.

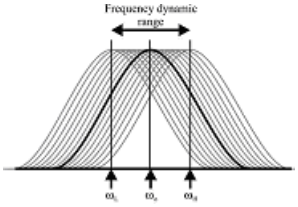

Fig 1: According to tissue deformation, the harmonic peak in the k_z direction will shift around the original frequency in proportion to local strain.

b. **Tagging and Tuning Frequency**: Given the targets minimum and maximum strain values $\varepsilon_{min}, \varepsilon_{max}$ and using Eq (2) and (3), it can be shown that the allowable values for ω_0 are bounded by:

$$\omega_L \geq B \Rightarrow \omega_0 \geq B(1+\varepsilon_{min}), (2)$$

$$\omega_c \leq B(1+\varepsilon_{min})(1+\varepsilon_{max})/(\varepsilon_{max}-\varepsilon_{min}), (3)$$

The first condition eliminates the interference from the DC component in the k_z domain by restricting ω_0 to be away from the DC component. The second condition is related to the fact that the peak shifts due to local deformations should be within the two tunings range. Figure (2) shows the strain ranges for different (ω_L–ω_H) normalized by B, then we deduce that we can achieve the max allowable strain range for ω_L-ω_H=B, (4).

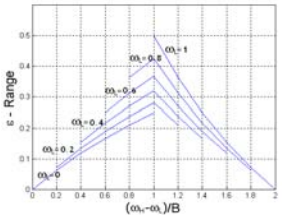

Fig 2: Maximum allowable strain range Vs. Difference between high and low tuning frequencies normalized to 1/slice thickness (B).

c. **Noise Effect:** 1. Due to the Rayleigh distribution in MRI Imaging, the low intensity values (as in the background) are more affected by the noise than higher intensity values. This creates a non-zero mean noise at pixels that are supposed to have zero values, which causes the allowable range for ω_L, ω_H to shrink. Also, due to the nonlinear nature of Eq. (1), the imposed noise on I_L and I_H affects the estimated strain values by changing the slope of the $\tilde{\varepsilon} - \varepsilon$ curve (Fig 3). This decrease in the slope degrades the accuracy of the estimated strain values. Hence, a small perturbation in the actual strain results in a major change in the corresponding estimated strain value).

Methods: Simulation for the noise effect is held by adding different noise level to the simulated slice profile then shifting the harmonic peak profile in the frequency domain for multiple steps and calculating the estimated strain for these shifts using (1). In order to verify the proposed relations and selection criteria, a SENC study was conducted using Philips 3T clinical scanner on a stationary liquid phantom to acquire multiple sets with different SNR. The strain curves for each pixel were calculated from each set. Given that the strain values should be zero inside the phantom, the effect of the noise was directly manifested. A normal volunteer was scanned to acquire multiple sets for a selected ω_0 but with different tuning frequencies to address their effect on the allowable strain range to measure. The strain curve for each voxel was plotted from the acquired sets.

Results: Fig. 3 shows the simulation results for the noise effect on the strain curve. As expected, higher noise levels decreases the dynamic range for estimating strain and lowers the slope of the curve; this leads to degradation in the strain measurements accuracy. At the worst case of SNR of 0.1, the estimated strain results become nearly constant regardless of the actual strain values. Fig 4 shows the bias effect for different SNR in the phantom study. Note that for reasonable SNR (SNR=4), the strain curve nearly shows the correct zero strain values while for low SNR set (SNR=0.5), an unacceptable large bias (~ 15%) can be observed. Fig 5 shows the effect of tuning selection on the allowable strain range in the myocardium. The whole strain range (0→-25%) appears in the curve that is acquired with the tuning calculated as in (4) while by decreasing the high tuning, the range begins to shrink. On the other hand, it does not begin to saturate directly following the full range curve. The reason is that lower values for high tuning produce images with better SNR, which delays the saturation of the strain curve.

Conclusion: An analysis for the accuracy of estimated strain values from noisy data using SENC technique was performed The effect of choices of tagging and tuning frequencies is discussed and an appropriate method for selecting these frequencies is introduced. Analysis of noise effect on the calculated strain values is discussed and verified via simulation and actual data.

References: [1] Nael F. Osman, "Imaging longitudinal cardiac strain on short-axis images using strain-encoded MRI," Magn. Resn. Med. 46: 324-10 (2001).

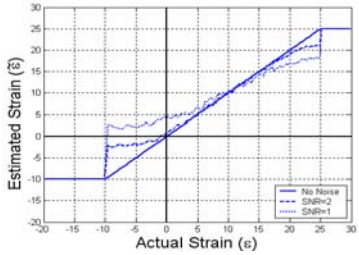

Fig 3: $\tilde{\varepsilon} - \varepsilon$ curve for sinc RF slice profile for different SNR. Note that the lower the SNR is, the narrower the strain range and the flatter the curve slope becomes.

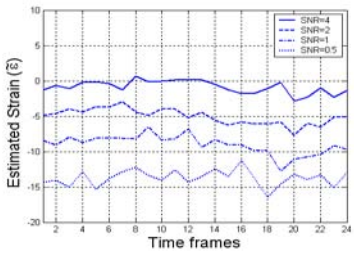

Fig 4: Strain curves for the same pixel in a stationary phantom (strain=0) from different data sets (each with different SNR). Note the bias increasing with SNR getting lower.

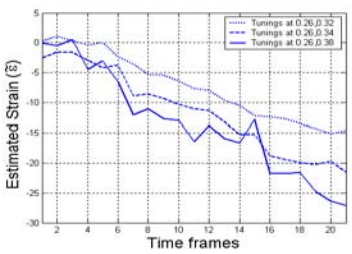

Fig 5: Strain curves for a pixel inside the myocardial tissue of a human subject. Each curve from a set acquired with different tuning parameters.